VIBRATION ANALYSIS OF LOW-ASPECT RATIO ROTATING BLADE MODELED AS A PLATE

Benyam Alaemayehu and Alem Bazezew
Department of Mechanical Engineering
Addis Ababa University

ABSTRACT

Vibration analysis of a low-aspect ratio blade modeled as a plate is presented which uses MATLAB coded computer program. The analysis presented employs an accurate strain-displacement relationship based on the thin plate theory, known as the Kirchhoff - Lava hypothesis. The equation of motion of the blade is derived using Kirchhoff - Lava plate theory, and the problem is solved by the finite element method, where rectangular plate elements with four nodes and three degrees of freedom for each node are utilized. A computer simulation of a numerical example is given to show the vibration characteristics of the rotating blade. Natural frequencies, corresponding mode shapes and the free vibration response are determined. Induced stresses related to the mode shapes are computed, and nature of these stresses are compared to actual data from the aviation industry.

Nomenclature

A	plate cross-sectional area
b	plate width
C	blade chord length
E	modulus of elasticity
G	shear modulus
h	plate thickness
$[K]$	system stiffness matrix
$[K]_e$	element stiffness matrix
L	plate length
M	moment
$[M]$	system mass matrix
$[M]_e$	element mass matrix
P	axial force due to rotation
Q	shear force
R	hub radius
x, y, z	moving coordinate system
Ω	angular velocity
ω	natural frequency
ρ	density of plate material
$(\ )^T$	transpose of a vector
$(\ )'$	differentiation with respect to spatial coordinate
$(\dot{\ })$	differentiation with respect to time

INTRODUCTION

In day-to-day industrial engineering activities, it is a common experience to come across turbomachines. These machines are vulnerable to major shutdowns, one of the causes being blade failures. And, it is known that vibration characteristics are significant factors in the safety, longevity and performance of rotating blade structures, especially for moving structures such as aerial propellers and turbomachinery blades. For economic and reliable design of rotating blade structures, it is necessary to estimate modal characteristics of those structures accurately. Since significant variation of modal characteristics result from rotational motion, the vibration analysis of turbomachinery blades has long been an intensive area of research. The first investigation of the vibrations of turbine blades was published by Campbell [1] in 1924. Problems of blade failure due to tangential mode vibrations were discussed and guidelines for avoiding blade resonance by de-tuning were proposed.

A number of researchers have used a cantilever beam model to analyse the vibration characteristics of turbine blades. Lo and Renbarger [2] developed equations of motion for a rotating cantilever beam, and concluded that vibration characteristics of a rotating beam are influenced by the orientation of the beam principal stiffness axes with respect to the plane of rotation. Their conclusion showed that the centrifugal stiffness predominantly increases the out of plane frequencies of the rotating cantilever beam than the in plane frequencies. Engida [5] used the finite element method to solve the rotating cantilever beam to determine the mode shapes and the natural frequencies.

Petricone and Sisto [3] used the Rayleigh-Ritz method to solve thin shell equations for natural frequencies and mode shapes of low aspect ratio, of twisted compressor blades mounted on a rigid base. Results were first obtained for flat cantilever plates of rectangular and skewed geometry which compared favorably with earlier data by Barton [3].

When blade length is small and sufficiently wide along its chord, which is the case in air craft

turbines, the blade behaves more like a plate or shell rather than a beam. Plate-like models are taken for lower aspect ratio blades, i.e. $L/C << 5$ and a low thickness-to-chord ratio, $h/C << 1$, where C is the cord length, h is the thickness of the blade and L is the length of the blade. Such blades have cross-sections that are subjected to deformations during vibration where the deflection(s) of any point on the blade is dependent on both its longitudinal and also its chord-wise position. Extensive research has been conducted to study vibration characteristics of turbine blades which include studies of a single or a group of blades using either discrete mass matrix methods or distributed mass studies, with or without finite element method.

To comprehend vibration characteristics of plates and provide accurate data for engineering applications, extensive research has been carried out employing different numerical methods such as the finite element method (FEM), Rayleigh-Ritz method (RRM), etc. that are based on Kirchhoff-Love theory, with first-order and higher-order shear deformation.

In this paper vibration analysis of low-aspect ratio blades, modeled as thin plate, is presented where an exact relationship between displacements and strains is derived using Newton's Law of motion. Also, an energy equilibrium equation was formulated by using the principle of virtual work, and the governing equation of the dynamic problem was solved by using the finite element method. A computer code is developed that employs the finite element method for analyzing the vibration characteristics of rotating blade to determine the natural frequencies and mode shapes of vibration. Stresses related to the mode shapes are also computed.

PROBLEM FORMULATION

Classical theory of plates involves certain approximations in order to simplify the problem to two dimensions. Such assumptions concern the linear variation of strains and stresses on lines normal to the plane of the plate. In deriving the governing equations of motion of a rotating cantilevered plate, the following assumptions are imposed.

1. Rotational speed of the plate is assumed to be constant.
2. The plate is homogenous and has isotropic material properties.
3. The blade has a low aspect ratio $L/C << 5$, and a low thickness-to-chord ratio $t/C << 1$. This assumption leads to the following simplifications.
   a. The plate is thin with thickness h and possesses a mean plane with planes for the external layers of the plate defined by $z = \pm\frac{1}{2}h$.
   b. Only the transverse displacement w is considered.
   c. The stress on the external layers is zero, and since the plate is thin, it is natural to assume that it vanishes for all z. i.e. the stress σ_z in the transverse direction is zero.
   d. Cross sections, initially normal to the mean plane, remain plane and orthogonal to it, implying that the transverse shear strains ε_{xz} and ε_{yz} are neglected.
   e. The displacements u and v in the $x-y$ plane result from two effects:
      - an initial displacement field, uniform over the thickness and resulting from loading of the plate in its plane behavior; and
      - a displacement field due to rotation of the cross section.
   f. Pre-twist rate of the blade along its longitudinal axis is uniform.
   g. There are no external forces that act on the blade.

EQUATION OF MOTION

The blade modeled as a cantilevered plate is shown in Fig. 1.a. The plate of length L, width b, and thickness h is attached to a rigid hub of radius R and at a stagger angle θ. Plate material properties are: Young's modulus E; shear modulus G; mass per unit area ρ; and Poisson's ratio ν. Neglecting transverse shear and rotary inertia effects in the problem formulation, Kirchhoff hypothesis is employed to derive the equation of motion. The *x-y-z* coordinate system, defined by the unit vectors ***i***, ***j***, and ***k***, respectively, is attached to the plate as shown in Fig. 1.a. The reference frame (the rigid hub) that passes through O is assumed to rotate at a constant angular speed Ω. A more general configuration of a plate having nonzero staggering angle can be obtained by rotating the plate around ***i*** axis.

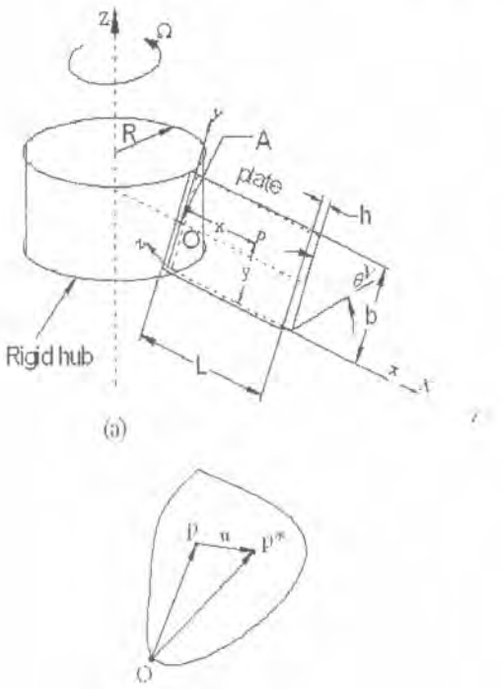

Figure 1 Configuration of a cantilever plate attached to a rigid hub at stagger angle θ

For the case of a rectangular plate in rotational motion, the dynamic load acting is determined from the acceleration distribution, and the resulting inertia force. Considering the elastic deformation of the plate, the position of a generic point p from the reference point is shown in Fig. 1.b. The elastic deformation of the plate causes the point p to move to p^* where the displacement vector $\boldsymbol{u}$ represents the elastic displacement. Considering only transverse deformation,

$$\boldsymbol{u} = w\boldsymbol{k}$$

The position vector of p^* with respect to the reference point O is given by

$$\boldsymbol{p}^* = x\boldsymbol{i} + y\boldsymbol{j} + w\boldsymbol{k} \tag{1}$$

The angular velocity of the reference frame is

$$\boldsymbol{\omega} = \Omega(\sin\theta\, \boldsymbol{j} + \cos\theta\, \boldsymbol{k})$$

and the velocity and acceleration of the reference point O of the coordinate system are given by

$$\begin{aligned} \boldsymbol{v}_A &= R\Omega(\cos\theta\, \boldsymbol{j} - \sin\theta\, \boldsymbol{k}) \\ \boldsymbol{a}_A &= -R\Omega^2\, \boldsymbol{i} \end{aligned} \tag{2}$$

Given these quantities, the velocity and acceleration of the arbitrary point p^* on the plate can be computed as

$$\boldsymbol{v}_{p^*} = \boldsymbol{v}_A + (\boldsymbol{\omega}_A \times \boldsymbol{p}^*) \tag{3}$$

$$\boldsymbol{a}_{p^*} = \boldsymbol{a}_A + \boldsymbol{\omega}_A \times (\boldsymbol{\omega}_A \times \boldsymbol{p}^*) \tag{4}$$

where $\boldsymbol{v}_A$ and $\boldsymbol{a}_A$ are the velocity and acceleration of point O, which is the reference point, fixed in the rigid frame A ; and p^* is the position vector from O to p^*.

Substituting for $\boldsymbol{p}^*$ and $\boldsymbol{\omega}$ in Eq. (4), the acceleration of point p^*, after simplifications, is

$$\mathbf{a}_{p^*} = \Omega^2 \begin{Bmatrix} -[(R+x)]\mathbf{i} + [w\sin\theta\cos\theta - y\cos^2\theta]\mathbf{j} \\ +[w\sin^2\theta - y\cos\theta\sin\theta]\mathbf{k} \end{Bmatrix} \tag{5}$$

Consider the rectangular plate subjected to a centrifugal force $P(x, y)$, whose components are P_x and P_y along the x - and y axes, respectively, as shown in Fig. 2.

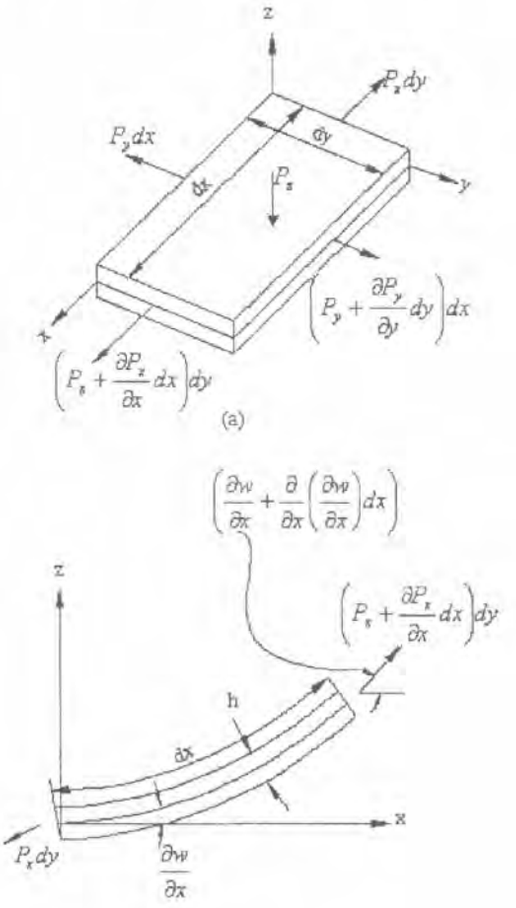

Figure 2 In-plane forces on a plate element

Due to the elastic deformation of the plate, the z component of P_x, for a small slope, is

$$P_z' = \frac{1}{dxdy}\left[\left(P_x + \frac{\partial P_x}{\partial x}dx\right)dy\left(\frac{\partial w}{\partial x} + \frac{\partial^2 w}{\partial x^2}dx\right) - P_x dy\frac{\partial w}{\partial x}\right] \tag{6}$$

where the slope is $\left(\frac{\partial w}{\partial x} + \frac{\partial}{\partial x}\left(\frac{\partial w}{\partial x}\right)dx\right)$ as shown in Fig. 2 b. Simplifying and neglecting higher order terms, the force per unit plate area in the z direction due to P_x is

$$P_z' = P_x\frac{\partial^2 w}{\partial x^2} + \frac{\partial P_x}{\partial x}\frac{\partial w}{\partial x} \tag{7}$$

Similarly, the force per unit plate area in the z direction due to P_y is

$$P_z'' = P_y\frac{\partial^2 w}{\partial y^2} + \frac{\partial P_y}{\partial y}\frac{\partial w}{\partial y} \tag{8}$$

Assuming that there is no in-plane stretch and no applied surface shear stresses, in the $x-$ and $y-$ directions, it follows that

$$\frac{\partial P_x}{\partial x} = 0 \qquad \frac{\partial P_y}{\partial y} = 0 \tag{9}$$

The centrifugal force is given by:

$$\mathbf{P}(x,y) = \rho\Omega^2\left\{\begin{array}{l}\left[R(L-x) + \frac{1}{2}\left(L^2 - x^2\right)\right]\mathbf{i} + \\ \left[\frac{1}{2}\left(b^2 - y^2\right)\cos^2\theta - (b-y)w\sin\theta\cos\theta\right]\mathbf{j} \\ + \left[y\cos\theta\sin\theta - w\sin^2\theta\right]\mathbf{k}\end{array}\right\} \tag{10}$$

Therefore, the x and y components of the centrifugal force are,

$$P_x = \rho\Omega^2\left[R(L-x) + \frac{1}{2}\left(L^2 - x^2\right)\right]$$

$$P_y = \rho\Omega^2\left[\frac{1}{2}\left(b^2 - y^2\right)\cos^2\theta - (b-y)w\sin\theta\cos\theta\right] \tag{11}$$

Applying Newton's law of motion in the z direction, and taking the z component of Eq.(5), the inertia force per unit area is:

$$P_z = \rho\left(a_{P^*}\right)_z = \rho\Omega^2\left(w\sin^2\theta - y\cos\theta\sin\theta\right) \tag{12}$$

From dynamic equilibrium of the plate, it has been determined that [10] the equation of motion can be represented as

$$\frac{Eh^3}{12(1-\nu^2)}\left[\left(\frac{\partial^4 w}{\partial x^4} + 2\frac{\partial^4 w}{\partial x^2\partial y^2} + \frac{\partial^4 w}{\partial y^4}\right)\right] + \frac{\partial}{\partial x}\left(P_x\frac{\partial w}{\partial x}\right) + \frac{\partial}{\partial y}\left(P_y\frac{\partial w}{\partial y}\right) + \rho h\frac{\partial^2 w}{\partial t^2} - P_z = F(x,y,t) \tag{13}$$

where $F(x,y,t)$ is the forcing function.

Substituting Eqs. (11) and (12) into Eq. (13) and simplifying yields

$$\frac{Eh^3}{12(1-\nu^2)}\left[\frac{\partial^4 w}{\partial x^4} + 2\frac{\partial^4 w}{\partial x^2\partial y^2} + \frac{\partial^4 w}{\partial y^4}\right] + \rho A\Omega^2 \left\{\begin{array}{l}\left[R(L-x) + \frac{L^2}{2}\left(1 - \frac{x^2}{L^2}\right)\right]\frac{\partial^2 w}{\partial x^2} + \\ \left[y w\sin\theta\cos\theta + \frac{b^2}{2}\left(1 - \frac{y^2}{b^2}\right)\cos^2\theta\right]\frac{\partial^2 w}{\partial y^2} + \\ y\cos\theta\sin\theta - w\sin^2\theta\end{array}\right\} = F(x,y)f(t) \tag{14}$$

This is the equation of motion in the transverse direction as a function of angular velocity and the stagger angle for the Kirchhoff – Lava plate.

FINITE ELEMENT SOLUTION OF THE EQUATION OF MOTION

The governing partial differential equation of motion given by Eq. (14) is solved by the finite element method. The finite element equations are obtained from the application of the virtual work equation, that is, from a weak formulation of the governing differential equation. To solve the problem, a rectangular element is used, with sides of length l_e and b_e having the nodes shown in Fig.3. The element nodal displacements are the transverse displacement w_j and the rotations $\phi_j = -\frac{\partial w_j}{\partial x}$ and $\psi_j = \frac{\partial w_j}{\partial y}$, $j = 1, 2, 3, 4$. The displacements w_j are in the z-direction; φ_j and ψ are positive (i.e. clockwise) rotations about the y- and x-axes, respectively. These definitions cause the negative sign in the relation between φ and $\partial w/\partial x$.

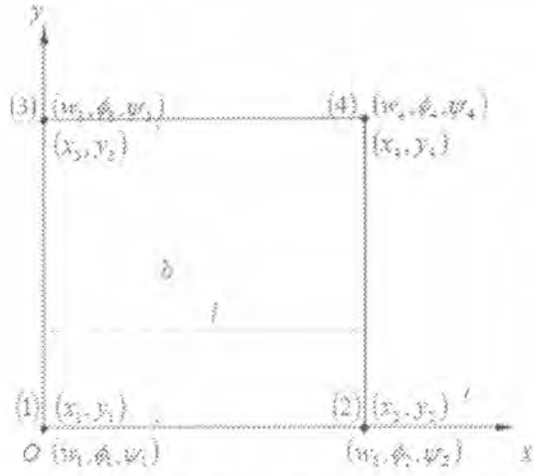

Figure 3 Rectangular element for element of a plate

The weak formulation using the virtual work method has been undertaken [6], and the equation of motion in the transverse direction has been derived as a function of angular velocity Ω, stagger angle θ, and shape functions. Thus, the equation of motion of the blade modeled as a Kirchhoff – Lava plate is

$$\sum_{j=1}^{\mu}\left[M_{ij}\ddot{q}_j + K_{ij}^{B}q_j + \Omega^2 K_{ij}^{GX2}q_j + \Omega^2\cos^2\theta\, K_{ij}^{GY2}q_j + R\Omega^2 K_{ij}^{GX1}q_j + \Omega^2\cos\theta\sin\theta\, M_{ij}q_j - \Omega^2\sin^2\theta\, M_{ij}q_j\right]=0 \quad (15)$$

where

$q_j = \begin{bmatrix} w_j \\ \varphi_j \\ \psi_j \end{bmatrix}$ are the nodal displacements;

$M_{ij} = \int_{-b/2}^{b/2}\int_{0}^{L}\rho N_i N_j\,dxdy$ are the nodal masses,

and the various terms of the stiffness matrix are:

$$K_{ij}^{B} = \frac{Eh^3}{12(1-\nu^2)}\int_{-b/2}^{b/2}\int_{0}^{L}\left[\left(\frac{\partial^2 N_i}{\partial x^2}\right)\left(\frac{\partial^2 N_j}{\partial x^2}\right)+\left(\frac{\partial^2 N_i}{\partial y^2}\right)\left(\frac{\partial^2 N_j}{\partial y^2}\right)+\nu\left(\frac{\partial^2 N_i}{\partial x^2}\right)\left(\frac{\partial^2 N_j}{\partial y^2}\right)+\nu\left(\frac{\partial^2 N_i}{\partial y^2}\right)\left(\frac{\partial^2 N_j}{\partial x^2}\right)+2(1-\nu)\left(\frac{\partial^2 N_i}{\partial x\partial y}\right)\left(\frac{\partial^2 N_j}{\partial x\partial y}\right)\right]dxdy$$

$$K_{ij}^{GX1} = \int_{-b/2}^{b/2}\int_{0}^{L}\left[\rho(L-x)\left(\frac{\partial N_i}{\partial x}\right)\left(\frac{\partial N_j}{\partial x}\right)\right]dxdy$$

$$K_{ij}^{GX2} = \frac{1}{2}\int_{-b/2}^{b/2}\int_{0}^{L}\left[\rho(L^2-x^2)\left(\frac{\partial N_i}{\partial x}\right)\left(\frac{\partial N_j}{\partial x}\right)\right]dxdy$$

$$K_{ij}^{GY2} = \frac{1}{2}\int_{-b/2}^{b/2}\int_{0}^{L}\left[\rho\left(\frac{b^2}{4}-y^2\right)\left(\frac{\partial N_i}{\partial y}\right)\left(\frac{\partial N_j}{\partial y}\right)\right]dxdy$$

The displacement w_j is approximated by the polynomial expression

$$w_j = a_1 + a_2x + a_3y + a_4x^2 + a_5xy + a_6y^2 + a_7x^3 + a_8x^2y + a_9xy^2 + a_{10}y^3 + a_{11}x^3y + a_{12}xy^3$$

or, $w_j = [X]\{a\}$ (16)

where $[X]$ is the row matrix of polynomial terms and the vector $\{a\}$ contains the coefficients a_i. From the assumed nodal displacements w_j the displacements q_j can be determined.

Considering the assumptions introduced in the problem formulation, the term in a_1 ensures rigid-body translation; those in a_2 and a_3 ensure rigid-body rotations; those in a_4 and a_6 ensure states of uniform curvature; and that in a_5 ensures a state of uniform twist. Thus the second and third conditions are satisfied. Since the virtual work contains second derivatives of the transverse displacement, w and its first derivatives should be continuous across element boundaries in order to satisfy the first condition and give conforming elements.

Along O_x, the displacement of the line joining nodes *1* and *2* in Fig. 3 is given by

$$w = a_1 + a_2x + a_4x^2 + a_7x^3$$

and

$$\phi = -\left[a_2 + 2a_4x + 3a_7x^2\right].$$

Thus the coefficients a_1, a_2, a_4 and a_7 are uniquely defined in terms of the four nodal values w_1, ϕ_1, w_2 and ϕ_2. As the latter are common to the two elements, for which O_x is a common boundary, there is continuity of w and ϕ across the inter-element boundary.

Also along O_x,

$$\psi = a_3 + a_5x + a_8x^2 + a_{11}x^3.$$

The values of ψ_1 and ψ_2 at nodes *1* and *2* are insufficient to define uniquely the four coefficients a_3, a_5, a_8 and a_{11}. As a consequence, there will not be continuity of the rotation ψ across element boundaries and this element is not conforming. Hence, as the mesh of elements, which represents a structure, is defined, convergence of eigenvalues to the correct values will not be monotonic.

Substituting nodal values of x and y in Eq. (16), and noting that the subscript e indicates the element matrix,

$$w_e = [w_1\ \phi_1\ \psi_1\ w_2\ \phi_2\ \psi_2\ w_3\ \phi_3\ \psi_3\ w_4\ \phi_4\ \psi_4]^T = N\{a\} \tag{17}$$

where

$$N = \begin{bmatrix}
1 & x_1 & y_1 & x_1^2 & x_1y_1 & y_1^2 & x_1^3 & x_1^2y_1 & x_1y_1^2 & y_1^3 & x_1^3y_1 & x_1y_1^3 \\
0 & -1 & 0 & -2x_1 & -y_1 & 0 & -3x_1^2 & -2x_1y_1 & y_1^2 & 0 & -3x_1^2y_1 & -y_1^3 \\
0 & 0 & 1 & 0 & x_1 & 2y_1 & 0 & x_1^2 & 2x_1y_1 & 3y_1^2 & x_1^3 & 3x_1y_1^2 \\
1 & x_2 & y_2 & x_2^2 & x_2y_2 & y_2^2 & x_2^3 & x_2^2y_2 & x_2y_2^2 & y_2^3 & x_2^3y_2 & x_2y_2^3 \\
0 & -1 & 0 & -2x_2 & -y_2 & 0 & -3x_2^2 & -2x_2y_2 & y_2^2 & 0 & -3x_2^2y_2 & -y_2^3 \\
0 & 0 & 1 & 0 & x_2 & 2y_2 & 0 & x_2^2 & 2x_2y_2 & 3y_2^2 & x_2^3 & 3x_2y_2^2 \\
1 & x_3 & y_3 & x_3^2 & x_3y_3 & y_3^2 & x_3^3 & x_3^2y_3 & x_3y_3^2 & y_3^3 & x_3^3y_3 & -y_3^3 \\
0 & -1 & 0 & -2x_3 & -y_3 & 0 & -3x_3^2 & -2x_3y_3 & y_3^2 & 0 & -3x_3^2y_3 & -y_3^3 \\
0 & 0 & 1 & 0 & x_3 & 2y_3 & 0 & x_3^2 & 2x_3y_3 & 3y_3^2 & x_3^3 & 3x_3y_3^2 \\
1 & x_4 & y_4 & x_4^2 & x_4y_4 & y_4^2 & x_4^3 & x_4^2y_4 & x_4y_4^2 & y_4^3 & x_4^3y_4 & -y_4^3 \\
0 & -1 & 0 & -2x_4 & -y_4 & 0 & -3x_4^2 & -2x_4y_4 & y_4^2 & 0 & -3x_4^2y_4 & -y_4^3 \\
0 & 0 & 1 & 0 & x_4 & 2y_4 & 0 & x_4^2 & 2x_4y_4 & 3y_4^2 & x_4^3 & 3x_4y_4^2
\end{bmatrix}$$

The coefficients a_i, $i = 1, 2, 3, \ldots, 12$ are obtained from

$$\{a\} = N^{-1}w_e = Bw_e \tag{18}$$

It is now possible to write the expression for the displacement within the element in a standard form as

$$w = [X]B\,w_e \tag{19}$$

where,

$$[X] = [1\ \ x\ \ y\ \ x^2\ \ xy\ \ y^2\ \ x^3\ \ x^2y\ \ xy^2\ \ y^3\ \ x^3y\ \ xy^3]$$

In Eq. (15), the bending strain energy expression can be re-arranged as follows:

$$K_{ij}^B = \frac{1}{2}\int_0^b\int_0^l \left\{ \begin{bmatrix} \partial^2w/\partial x^2 & \partial^2w/\partial y^2 & 2\partial^2w/\partial x\partial y \end{bmatrix} \overline{D} \begin{bmatrix} \partial^2w/\partial x^2 \\ \partial^2w/\partial y^2 \\ 2\partial^2w/\partial x\partial y \end{bmatrix} \right\} dx\,dy \tag{20}$$

where

$$\overline{D} = \frac{Eh^3}{12(1-\nu^2)} \begin{bmatrix} 1 & \nu & 0 \\ \nu & 1 & 0 \\ 0 & 0 & \frac{1}{2}(1-\nu) \end{bmatrix}.$$

Therefore, from Eq. (15) the weak form of the governing equations for an element can be written as:

$$\int_0^b\int_0^l \begin{bmatrix} \partial^2w/\partial x^2 & \partial^2w/\partial y^2 & 2\partial^2w/\partial x\partial y \end{bmatrix} \overline{D} \begin{bmatrix} \partial^2w/\partial x^2 \\ \partial^2w/\partial y^2 \\ 2\partial^2w/\partial x\partial y \end{bmatrix} dx\,dy + \int_0^b\int_0^l \frac{\rho\Omega^2}{2}(l^2 - x^2)\left(\frac{\partial w}{\partial x}\right)^T\left(\frac{\partial w}{\partial x}\right)dx\,dy +$$

$$\int_0^b\int_0^l \frac{\rho\Omega^2\cos^2\theta}{2}(b^2 - y^2)\left(\frac{\partial w}{\partial y}\right)^T\left(\frac{\partial w}{\partial y}\right)dx\,dy + \int\int R\rho\Omega^2(l - x)\left(\frac{\partial w}{\partial x}\right)^T\left(\frac{\partial w}{\partial x}\right)dx\,dy +$$

$$\int_0^b\int_0^l \left(\rho\Omega^2\cos\theta\sin\theta(w)^T w - \rho\Omega^2\sin^2\theta(w)^T w\right)dx\,dy = 0 \tag{21}$$

From Eq. (16) we have

$$\begin{bmatrix} \partial^2w/\partial x^2 \\ \partial^2w/\partial y^2 \\ 2\partial^2w/\partial x\partial y \end{bmatrix} = \begin{bmatrix} 0 & 0 & 0 & 2 & 0 & 0 & 6x & 2y & 0 & 0 & 6xy & 0 \\ 0 & 0 & 0 & 0 & 0 & 2 & 0 & 0 & 2x & 6y & 0 & 6xy \\ 0 & 0 & 0 & 0 & 2 & 0 & 0 & 4x & 4y & 0 & 6x^2 & 6y^2 \end{bmatrix} \{a\} = \overline{X}Bw_e \tag{22}$$

$$\frac{\partial w}{\partial x}=\begin{bmatrix}0 & 1 & 0 & 2x & y & 0 & 3x^2 & 2xy & y^2 & 0 & 3x^2y & y^3\end{bmatrix}\{a\}=\left(\frac{\partial N}{\partial x}\right)Bw_e \tag{23}$$

$$\frac{\partial w}{\partial y}=\begin{bmatrix}0 & 0 & 1 & 0 & x & 2y & 0 & x^2 & 2xy & 3y^2 & x^3 & 3xy^2\end{bmatrix}\{a\}=\left(\frac{\partial N}{\partial y}\right)Bw_e \tag{24}$$

where

$$[\overline{X}]=\begin{bmatrix}0 & 0 & 0 & 2 & 0 & 0 & 6x & 2y & 0 & 0 & 6xy & 0\\ 0 & 0 & 0 & 0 & 0 & 2 & 0 & 0 & 2x & 6y & 0 & 6xy\\ 0 & 0 & 0 & 0 & 2 & 0 & 0 & 4x & 4y & 0 & 6x^2 & 6y^2\end{bmatrix}$$

$$\left(\frac{\partial N}{\partial x}\right)=\begin{bmatrix}0 & 1 & 0 & 2x & y & 0 & 3x^2 & 2xy & y^2 & 0 & 3x^2y & y^3\end{bmatrix}$$

$$\left(\frac{\partial N}{\partial y}\right)=\begin{bmatrix}0 & 0 & 1 & 0 & x & 2y & 0 & x^2 & 2xy & 3y^2 & x^3 & 3xy^2\end{bmatrix}$$

Using Eqs. (16), and (21) through (23) in Eq. (20), the potential energy is given by

$$V_e=\frac{1}{2}w_e^T K_e w_e \tag{25}$$

where the element stiffness matrix is

$$K_e=B^T\left[\int_0^l\int_0^b\begin{bmatrix}\overline{X}^T\overline{D}\,\overline{X}+\frac{\rho\Omega^2}{2}\left[\left(l^2-x^2\right)+2R(l-x)\right]\left(\frac{\partial N}{\partial x}\right)^T\left(\frac{\partial N}{\partial x}\right)+\\ \frac{\rho\Omega^2}{2}\cos^2\theta\left(b^2-y^2\right)\left(\frac{\partial N}{\partial y}\right)^T\left(\frac{\partial N}{\partial y}\right)+\rho\Omega^2\cos\theta\sin\theta[X]^T[X]-\\ \rho\Omega^2\sin^2\theta[X]^T[X]\end{bmatrix}dx\,dy\right]B \tag{26}$$

The kinetic energy of the element is given by

$$T_e=\frac{1}{2}\int_0^l\int_0^b\rho h\left(\partial w/\partial t\right)^2\,dy\,dx \tag{27}$$

From Eq. (12) and (13) we get

$$\frac{\partial w}{\partial t}=[X]B\,\dot{w}_e \tag{28}$$

Therefore, the kinetic energy is obtained to be

$$T_e=\frac{1}{2}\dot{w}_e^T M_e\dot{w}_e \tag{29}$$

where the element mass matrix is

$$M_e=B^T\left[\int_0^l\int_0^b[X]^T\rho h[X]dy\,dx\right]B \tag{30}$$

Thus, the equation of motion given by Eq. (11) is reduced to

$$[M]\{\ddot{w}\}+[K]\{w\}=0 \tag{31}$$

where $[M]$ and $[K]$ are $n\times n$ global mass and stiffness matrices, respectively, assembled from the element matrices; and $\{w\}$ is $n\times 1$ displacement vector.

EIGENSOLUTION

The material used for this analysis is a titanium alloy Ti-6AL-4V. This material has numerous applications in the aerospace industry, particularly in turbine blades. The material properties for Ti-6AL-4V and the dimensions of the plate considered are given in Table 1. The dimensions are approximations of an actual turbine blade used in BOEING engines.

Table 1: Material properties of Titanium alloy (Ti-6Al-4V) and plate dimensions

Property	Symbol	value
density	ρ	$3000\ kg/m^3$
Young's modulus	E	$1.14\times10^{11}\ Pa$
Poisson's ratio	ν	0.33
Thickness	t	$0.0025m$
Length	l	$0.04m$
Width	b	$0.04m$

A code in MATLAB was written to solve the eigenvalue problem described by the equation of motion (31). The results of the eigensolution for the square plate are presented in Figs. 4-7 which show the mode shapes and the stresses induced for the first four modes. The effect of the stagger angle θ on the natural frequencies is also studied and the results are given in Table 2. Table 3 indicates the influences of hub radius on the natural frequencies in which the results are expressed in non-dimensional form.

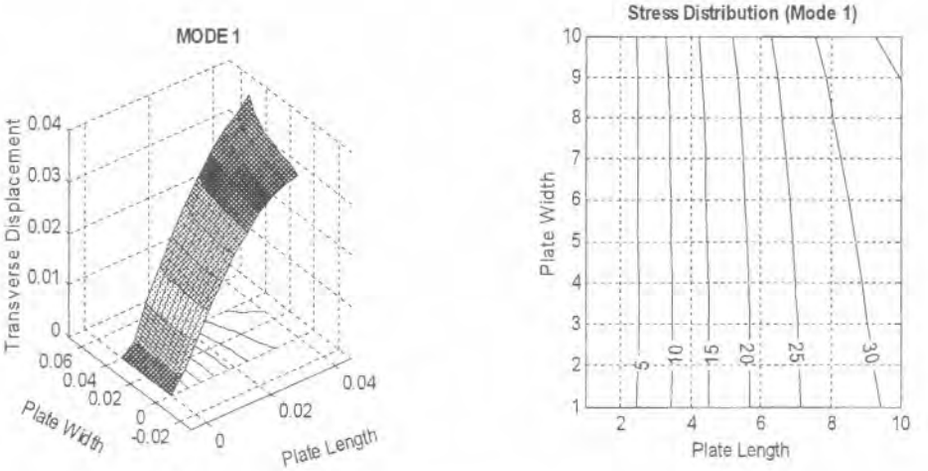

Figure 4 (a) Modal shape and (b) stress distribution for mode 1

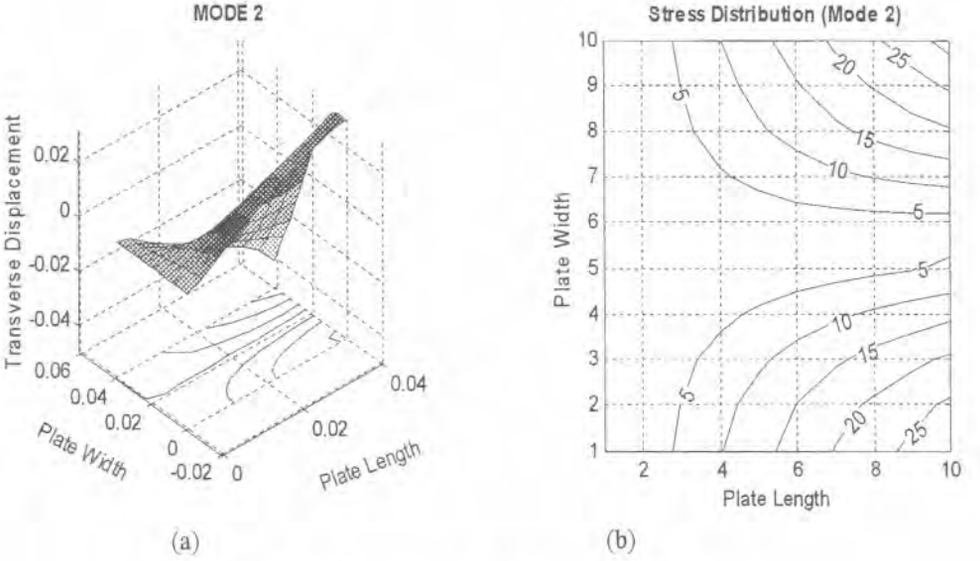

Figure 5 (a) Modal shape and (b) stress distribution for mode 2

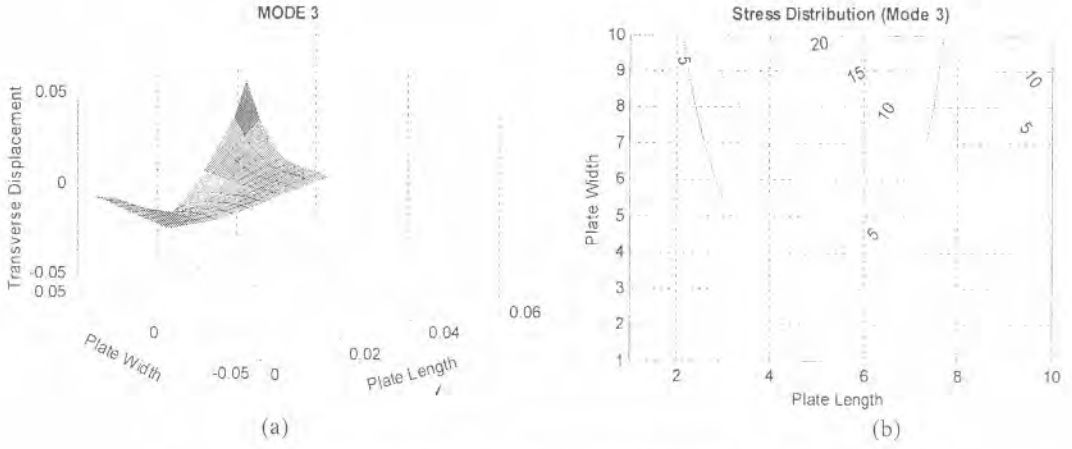

Figure 6. (a) Modal shape and (b) stress distribution for mode 3

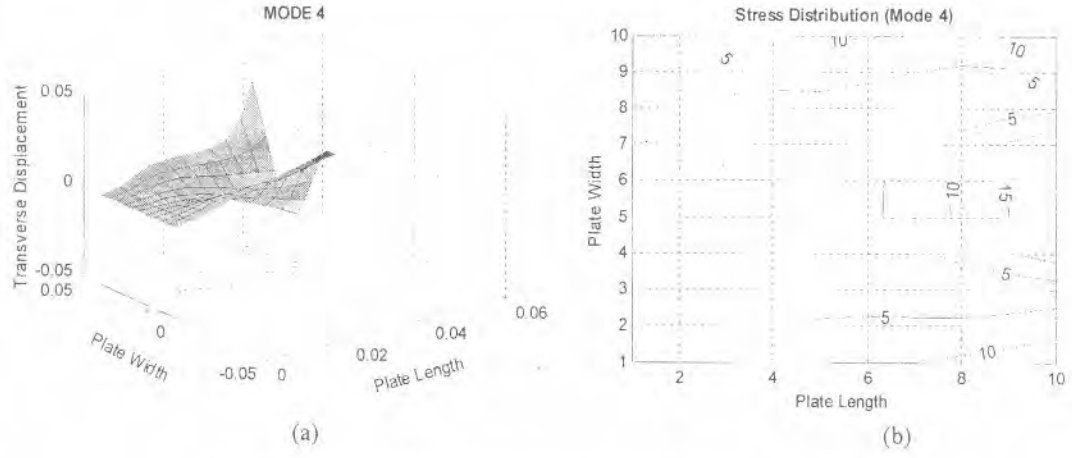

Figure 7 (a) Modal shape and (b) stress distribution for mode 4

Table 2: Effect of stagger angle θ on the non-dimensional natural frequency

Mode	Stagger angle θ				
	0°	15°	30°	45°	60°
1	3.9483	3.7925	3.6646	3.0555	3.0254
2	8.3690	6.4606	4.9187	4.5766	4.5148
3	11.1535	11.1383	9.2867	6.8404	4.8281
4	13.6092	13.2263	10.6806	7.6320	5.2112

Table 3: Effect of hub radius on the non-dimensional natural frequencies

Hub Radius R	First Natural Frequency	Second Natural Frequency
0	3.9483	8.3690
0.04	17.2047	21.2620
0.4	36.6153	60.6307

Table 4: Effects of rotational speed on the first and second natural frequency

Rotational Speed (rpm)	First Natural Frequency (rpm)	Second Natural Frequency (rpm)
0	6,192	15,585
10,000	139,280	255,690
20,000	271,030	494,630

DISCUSSION OF RESULTS

a. *Mode shapes and stresses*: By examining the mode shapes of the plate given in Figs. 4 and 5, it can be hypothesized which mode will concentrate the highest energy at the point of interest, which is the middle point of the free-end. This is the point practically observed in blade failures. Knowing that

stress is a function of displacement, a mode will be chosen that shows the greatest rate of change of relative displacement of the plate near the midpoint of the free-end. Mode 4 is selected as the mode that will concentrate the highest energy at the center point of the tip of the plate. Modes 1 and 2 will impart little energy at the desired point since the edge is undeformed. Mode 3 will impart a little energy since the relative displacement is so small.

b. *Stagger angle* θ : The results obtained in this paper indicate that the effect of the stagger angle on the non-dimensional natural frequency to be significant as can be seen from Table 2.

c. *Hub radius*: Table 3 indicates that the non-dimensional natural frequencies increase with increasing hub radius. Increase in hub radius results in increased centrifugal forces which introduce higher tension, thus stiffening the blade more. As a consequence, the natural frequencies in bending modes increase.

d. *Rotational speed*: Table 4 indicates that the natural frequencies increase with increasing rotational speed of the plate. As can be observed from Eq. (11), the additional term in the stiffness due to the rotational speed stiffens the blade more and as a result the natural frequencies increase.

The results obtained in (a) through (d) above, agree with the results obtained by other researchers, notably those of Rao [4] who has investigated blade vibrations extensively.

CONCLUSION

A numerical procedure for the analysis of vibration of rotating cantilever plates with stagger angle by Finite Element Method with an accurate strain-displacement relationship is proposed based on the Kirchhoff-Lava plate theory, in which rectangular plate elements with four nodes and three degrees of freedom for each node are utilized. A method employing assumed modes is used to obtain numerical results. It is shown that the rotating plate natural frequencies increase with the angular speed, that their increasing rates grow as the hub radius increases, and that the natural frequency loci are lowered by increasing the staggering angle. It is also found that some natural frequencies increase faster than others as the aspect ratio or the angular speed increases. This results in the phenomena of eigenvalue loci crossing and veering. When two loci cross, the corresponding two mode shapes are simply switched and remain nearly unchanged. When two loci veer, however, mode shape variations occur continuously in the veering region. It is also observed that the two continuously changing mode shapes. The results obtained are useful to investigators in that they may be used as a bench mark for future investigations of blade vibrations. And the program developed may be used to include other design characteristics by way of refining the blade modeling.

REFERENCES

[1] Campbell,W., "Tangential Vibration of Steam Turbine Buckets." *Trans. of ASME*, pp. 643 – 671, 1924.

[2] Lo, H.; Renbarger.J.L.; "Bending Vibration of a Rotating Beams." *Proc. 1st U.S. National Conference of Applied Mechanics, ASME*, pp. 75-79, 1977.

[3] Petricone, R. and Sisto, F.: "Vibration Characteristics of Low Aspect ratio Compressor Blades," *Journal of Engineering for Power*, Vol. pp. 1 – 10, 1971.

[4] Rao, J. S., *Turbomachine Blade Vibration*, New Age International (P). Limited, New Delhi, 1997.

[5] Dereje Engida: "Lateral Vibration of Rotating Cantilever Blade Modeled as Beam", *M. Sc. Thesis*, Faculty of Technology, Addis Ababa University, 2004.

[6] Benyam Alemayehu: "Vibration Analysis of a Low Aspect Ratio Turbine Blade Modeled as Plate", *M. Sc. Thesis*, Faculty of Technology, Addis Ababa University, 2005.